Supporting Information: Gradient of Non-Linear Cost Function

Minimizing Eq. (1) with a gradient-based technique requires calculating its gradient. An analytical formulation for $\nabla f = \left[\partial_{\boldsymbol{W}} f, \partial_{\boldsymbol{F}} f, \partial_{\boldsymbol{R}_2^*} f\right]$ of the data consistency term

$$f = \sum_{c,t_n} \| E(\boldsymbol{W}, \boldsymbol{F}, \boldsymbol{R}_2^*)_{c,t_n} - \boldsymbol{Y}_{c,t_n} \|_2^2 = \sum_{c,t_n} \| \boldsymbol{R}_{c,t_n} \|_2^2$$

can be derived following the description in (1). For simplification, $\boldsymbol{R}_{c,t_n}$ is used here to denote the data residual. The gradient with respect to water, fat, and R_2^* can then be calculated with

$$\frac{\partial f}{\partial \mathbf{W}} = \sum_{c,t_n} \mathrm{e}^{-\boldsymbol{R}_2^* t_n} \operatorname{Re}\left\{ \overline{\boldsymbol{C}_c}\, \mathrm{e}^{-2\pi i \boldsymbol{\Phi} t_n}\, \mathrm{FT}^{-1}\left(\boldsymbol{R}_{c,t_n}\right)\right\},$$

$$\frac{\partial f}{\partial \mathbf{F}} = \sum_{c,t_n} \mathrm{e}^{-\boldsymbol{R}_2^* t_n} \operatorname{Re}\left\{ \overline{\boldsymbol{C}_c}\, \mathrm{e}^{-2\pi i \boldsymbol{\Phi} t_n}\, \mathrm{FT}^{-1}\left(\overline{\boldsymbol{D}_{t_n}} \boldsymbol{R}_{c,t_n}\right)\right\},$$

and

$$\begin{aligned} \frac{\partial f}{\partial \boldsymbol{R}_2^*} = & \sum_{c,t_n} (-t_n)\, \mathrm{e}^{-\boldsymbol{R}_2^* t_n} \operatorname{Re}\left\{ \overline{\boldsymbol{C}_c}\, \mathrm{e}^{-2\pi i \boldsymbol{\Phi} t_n}\, \overline{\boldsymbol{W}}\, \mathrm{FT}^{-1}\left(\boldsymbol{R}_{c,t_n}\right)\right\} \\ & + \sum_{c,t_n} (-t_n)\, \mathrm{e}^{-\boldsymbol{R}_2^* t_n} \operatorname{Re}\left\{ \overline{\boldsymbol{C}_c}\, \mathrm{e}^{-2\pi i \boldsymbol{\Phi} t_n}\, \overline{\boldsymbol{F}}\, \mathrm{FT}^{-1}\left(\overline{\boldsymbol{D}_{t_n}} \boldsymbol{R}_{c,t_n}\right)\right\}. \end{aligned}$$

Here, $\overline{A}$ corresponds the complex conjugate of A, and $\mathrm{FT}^{-1}(.)$ performs an inverse non-uniform fast Fourier transform (NUFFT). For minimizing the ℓ_1 norm of the regularization terms, the reader is referred to (2).

References

1. Block KT, Uecker M, Frahm J. Model-based iterative reconstruction for radial fast spin-echo MRI. IEEE Trans Med Imag 2009;28(11):1759–1769.

2. Lustig M, Donoho D, Pauly JM. Sparse MRI: The application of compressed sensing for rapid MR imaging. Magn Reson Med 2007;58(6):1182–1195.

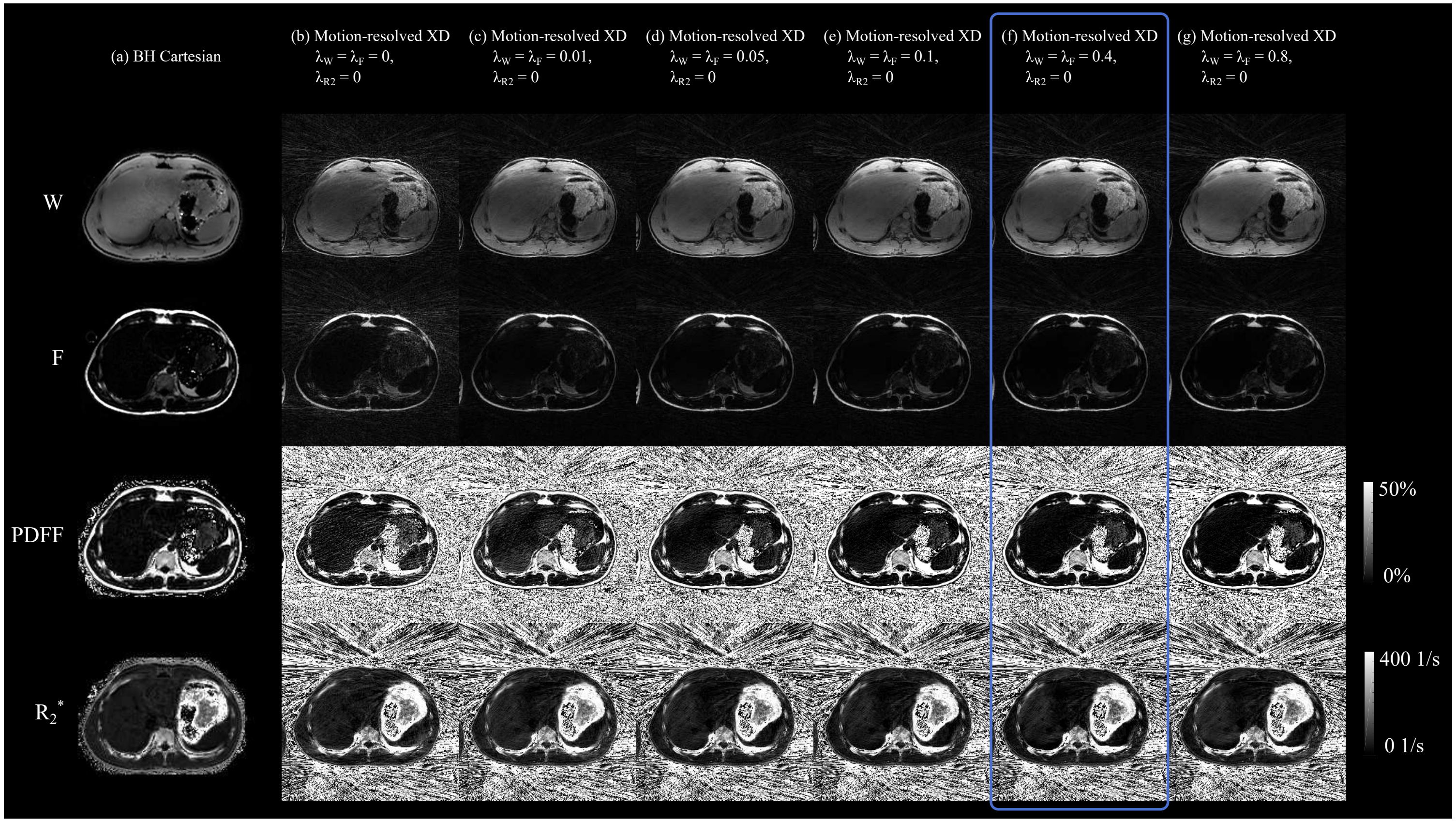

Supporting Information Figure S1. Effect of λ_W and λ_F regularization strength. In-vivo patient maps of (**a**) the Cartesian reference scan and (**b**)-(**g**) motion-resolved free-breathing maps for varying regularization weights λ_W, λ_F and $\lambda_{R_2^*} = 0$. Chosen λ_W and λ_F values are framed. The Dixon-RAVE sequence did not apply "prescan normalize", resulting in a noticeable intensity drop in the water and fat maps towards the center compared to BH Cartesian (noticable especially in the top row).

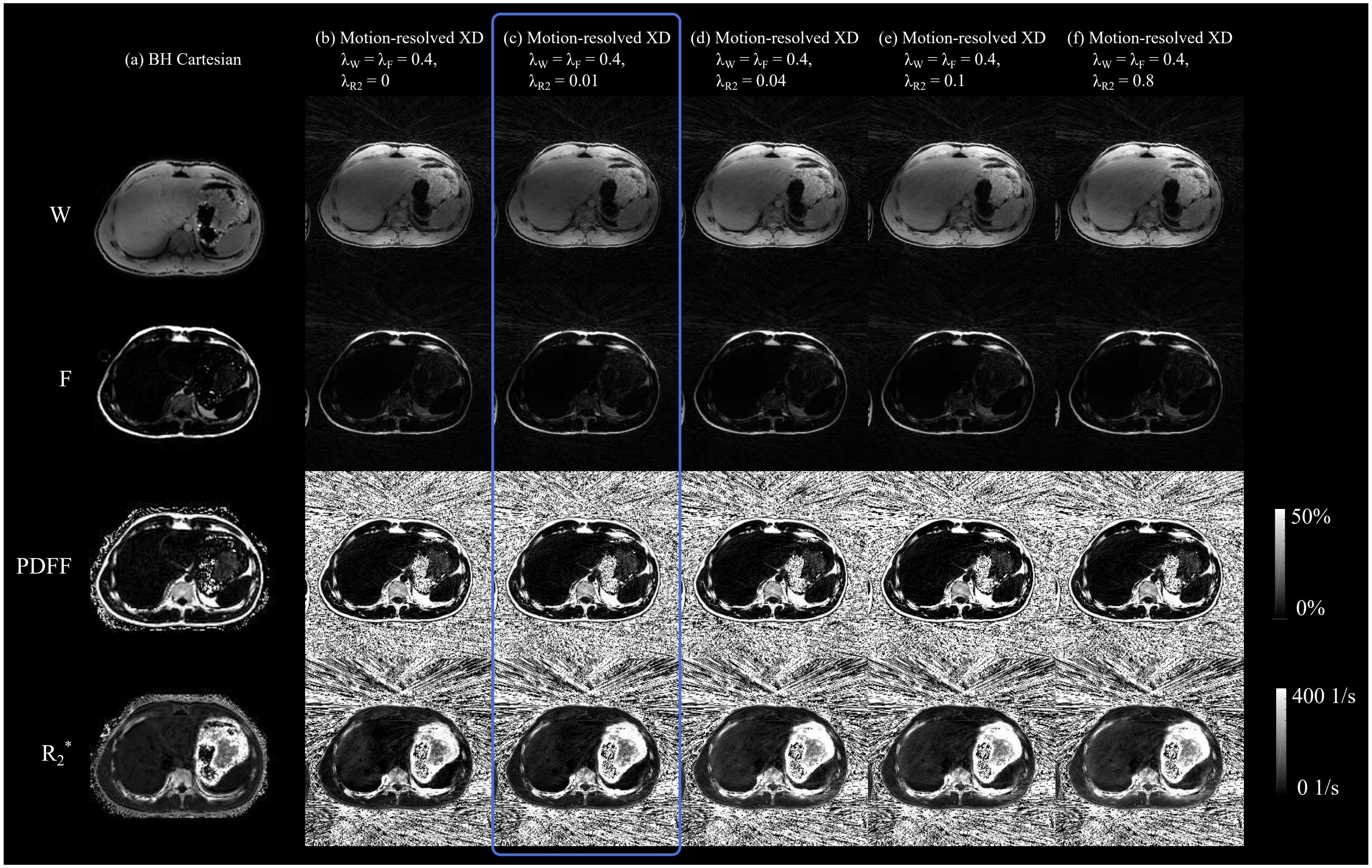

Supporting Information Figure S2. Effect of $\lambda_{R_2^*}$ regularization strength on motion-resolved maps. In-vivo patient maps from (**a**) Cartesian reference scan and (**b**)-(**g**) motion-resolved reconstruction for varying R_2^* regularization weights ($\lambda_W = \lambda_F = 0.4$). Maps of the chosen $\lambda_{R_2^*}$ value are framed. The Dixon-RAVE sequence did not apply “prescan normalize”, resulting in a noticeable intensity drop in the water and fat maps towards the center compared to BH Cartesian (noticable especially in the top row).

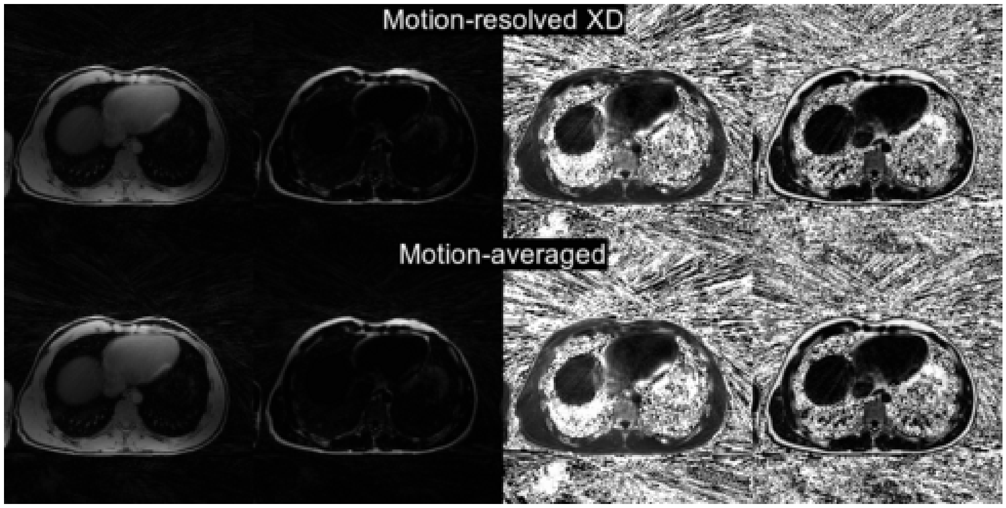

Supporting Information Figure S3. Example water, fat, R_2^*, and PDFF maps (from left to right) of the methods "Motion-resolved XD" (top) and "Motion-averaged" (bottom) from a patient (male, age: 25 years, weight: 78 kg, BMI: $24.6\,\mathrm{kg\,m^{-2}}$). This animation is additionally included in a separate file (SupplFig3.gif).

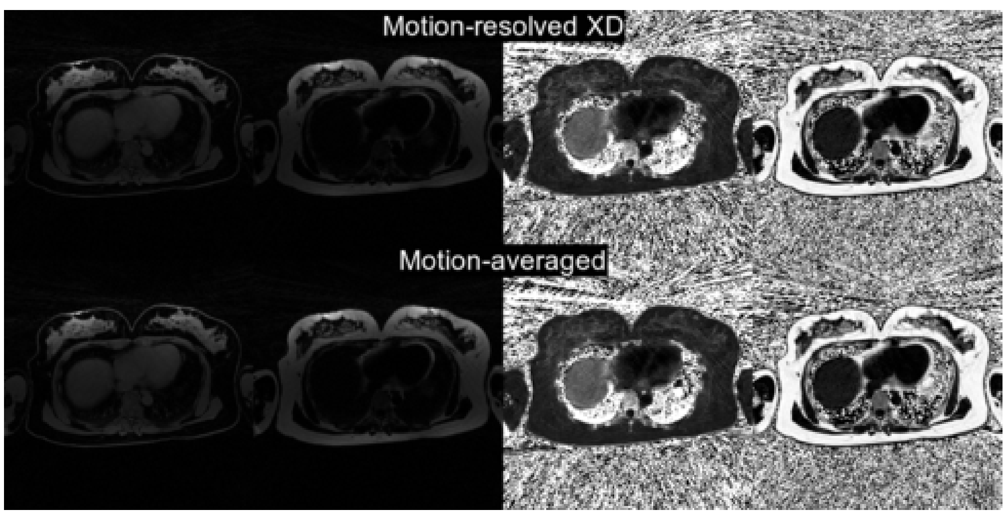

Supporting Information Figure S4. Example water, fat, R_2^*, and PDFF maps (from left to right) of the methods "Motion-resolved XD" (top) and "Motion-averaged" (bottom) for a patient (female, age: 50 years, weight: 59.9 kg, BMI: $24.1\,\mathrm{kg\,m^{-2}}$) with elevated PDFF and R_2^*. This animation is additionally included in a separate file (SupplFig4.gif).

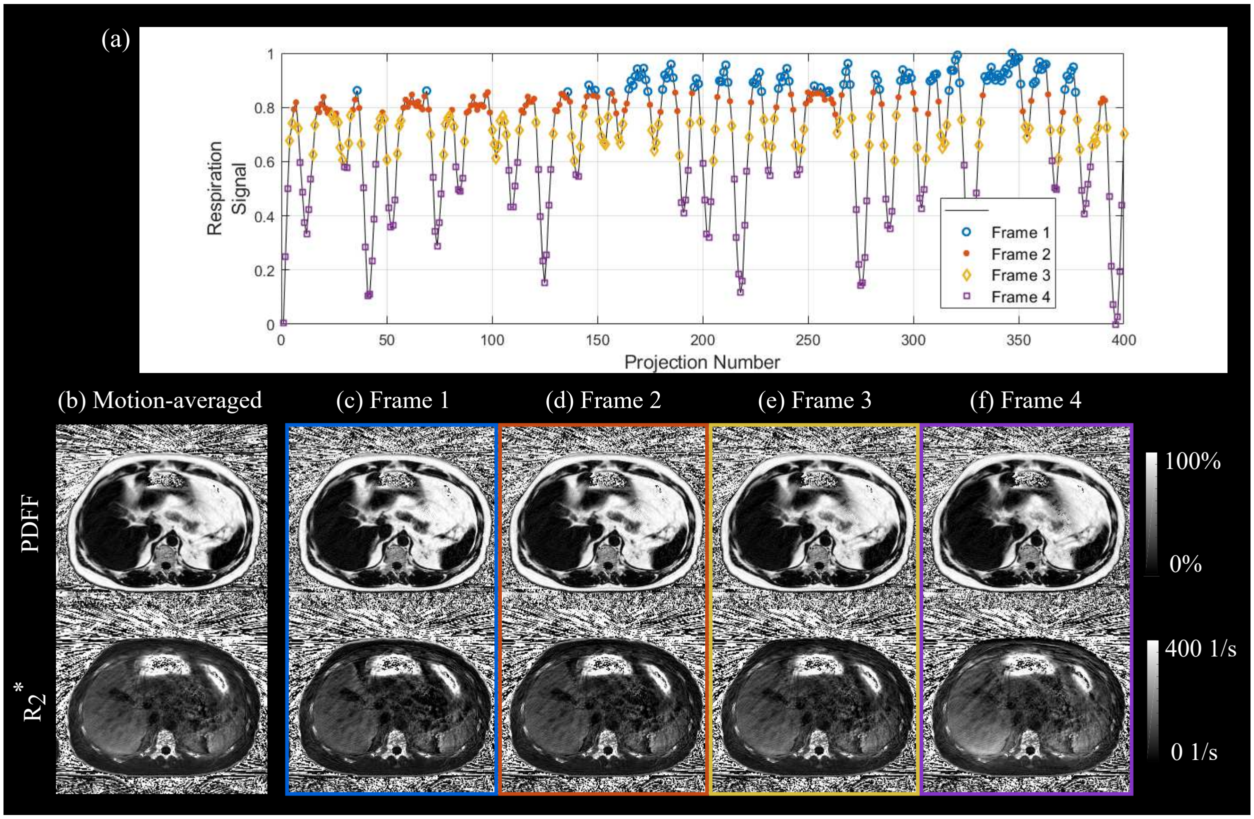

Supporting Information Figure S5. Estimated respiratory signal (**a**), and PDFF (top) and R_2^* (bottom) maps of a patient with slightly elevated R_2^* values, reconstructed using the motion-averaged reconstruction (**b**). Motion-resolved XD reconstruction for frame 1 (end-expiration) to frame 4 (end-inspiration) are shown in (**c**)-(**f**). The motion-resolved XD parameter maps corresponding to frame 2 are selected for quantitative evaluation.

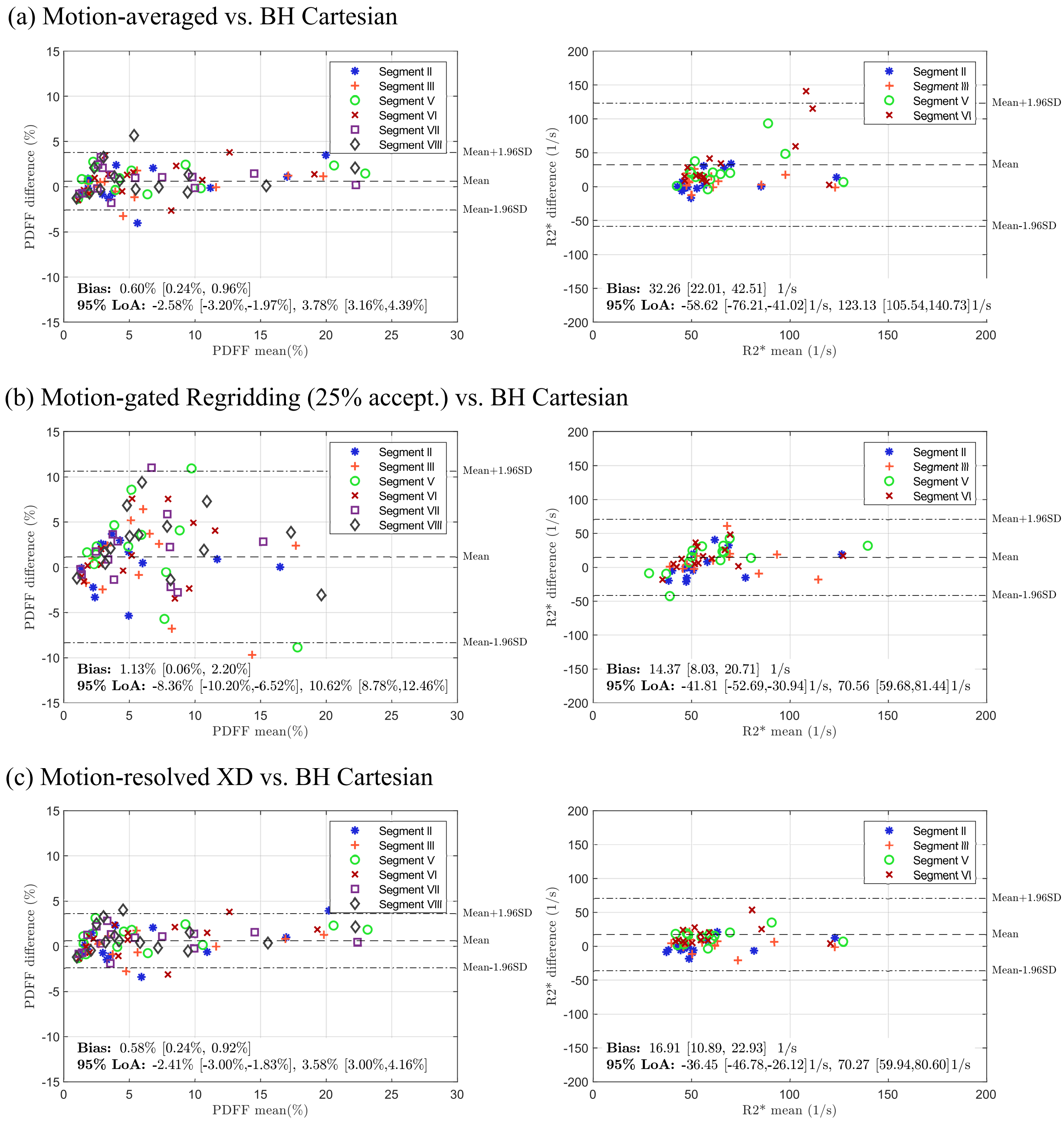

Supporting Information Figure S6. Bland-Altman plots for the measured (left) PDFF and (right) R_2^* values, depicting the agreement of (**a**) motion-averaged reconstructions to the Cartesian reference, (**b**) motion-gated ($25\,\%$ acceptance rate) reconstructions followed by regridding and image-based water/fat separation to the Cartesian reference, and (**c**) motion-resolved XD reconstructions to the Cartesian reference. The plots indicate overall biases, 95% LoA and their 95% confidence intervals.